Available online at www.sciencedirect.com
SCIENCE DIRECT®
ELSEVIER
Ocean Engineering 32 (2005) 623–650
OCEAN ENGINEERING
www.elsevier.com/locate/oceaneng

Wave kinematics factor in real and simulated storms

V. Venugopal*, J. Wolfram, B.T. Linfoot

School of the Built Environment, Heriot-Watt University, Edinburgh EH14 4AS, UK

Received 5 March 2004; accepted 14 July 2004
Available online 10 December 2004

Abstract

This paper presents wave kinematics factors (F_S)[1] for the storm data collected in the northern North Sea from three wave height altimeters mounted on a jacket platform. Directional wave spectra and spreading functions are computed from the surface elevation measurements of the storm data, from which wave kinematic factors are derived. The hybrid wave model of [Zhang, J., Yang, J., Wen, J., Prislin, I., Hong, K., 1999. Deterministic wave model for short-crested ocean waves. Part I. Theory and numerical scheme. Applied Ocean Research, 21, 167–188] is used to predict wave particle kinematics of the storm data and the predicted kinematics are also used to compute the wave kinematics factor. Experimental investigations have also been undertaken in a multidirectional wave basin, wherein the storms recorded at the platform are reproduced with a scale of 1:55. Wave elevations and wave particle velocities beneath the waves are measured in the wave basin for both long-crested and short-crested waves using arrays of wave probes and velocimeters and the measured wave kinematics are utilised to calculate the wave kinematics factor for the reproduced storms. The wave kinematic factors computed for the full-scale measurements compare well with the values for the reproduced storms in the wave basin. This investigation show that the wave kinematics factors vary with the spreading parameter s and for the northern North Sea the values, $F_s=0.78$ ($s=2$); $F_s=0.85$ ($s=4$); $F_s=0.88$ ($s=6$) and $F_s=0.92$ ($s=8$) are appropriate.

Keywords: Storm waves; Directional wave spectrum; Wave spreading; Wave kinematics factor; Second order wave kinematics

* Corresponding author. Tel.: +44 131 451 4421; fax: +44 131 451 4617.
E-mail address: v.venugopal@sbe.hw.ac.uk (V. Venugopal).

[1] Also known as wave spreading factor or kinematics reduction factor.

0029-8018/$ - see front matter
doi:10.1016/j.oceaneng.2004.07.009

1. Introduction

Short-crested waves result in smaller wave forces than unidirectional waves of equal spectral characteristics and this has been demonstrated in many laboratory studies (Aage et al., 1989; Hogedal et al., 1994; Chaplin et al., 1995). Understanding why and how the reduction of forces in a directional sea occurs, requires knowledge of the wave kinematics and its effects on structural loading. The peak particle velocities under waves become smaller as the waves become more spread and to account for this reduction in the kinematics a spreading factor (or kinematics reduction factor), which is the square root of the in-line variance ratio (Haring and Heideman, 1980), is applied (Heideman and Weaver, 1992; API, 1993; Jonathan et al., 1994; Tucker, 1996). The procedure to account for this reduction is to apply this spreading factor to the kinematics calculated from a unidirectional wave system in the design of fixed structures. The spreading factor is dependent on the type of storm in the region and the relative location of the storm centre (Forristall and Ewans, 1998). API (1993) recommended the spreading factor values in the range of 0.85–0.95 for tropical storms and 0.95–1.00 for extratropical storms and these values correspond to the spectral peak period. Forristall and Ewans (1998) recommended the spreading factor values, $\phi = 0.880$ for low-latitude monsoons, $\phi = 0.867$ for tropical cyclones and $\phi = 1.0193 - 0.00208|\lambda|$ for extratropical storms with $36 < |\lambda| < 72$ where λ is the latitude in degrees. They suggest that the spreading factor should be calculated considering the entire wave spectrum by integrating the velocity variances. Tucker (1996) analysed storm measurements from around the UK and suggests that two versions of the spreading factor definitions should be considered: one uses the energy weighted average ($F_{S2}(peak)_3$) over 0.03 Hz centred on the spectral peak and the second the energy weighted average ($F_{S2}(mean)$) over the entire spectrum. These values are calculated from the second angular harmonic of the wave spectrum. Tucker (1996) reported that the sites to the west of the UK gave $F_{S2}(peak)_3$ typically as 0.95 for extreme significant waves and some storms showed values as high as 0.97 or 0.98. The corresponding $F_{S2}(mean)$ was 0.90. However, clockwise round the UK, a number of storms showed lower values than above which is attributed to the combination of the proximity of the land and meteorological complexity. The present study contributes further information to the selection of appropriate spreading factors based on the analysis of several major storms recorded in the northern North Sea.

Storm wave data collected from the North Alwyn platform, in 130 m of water, in the northern North Sea has been analysed to determine the characteristics of real, extreme, three-dimensional waves. The evolution of wave characteristics during the rise, peak and decay of storms have been examined (Wolfram et al., 2001) and it has been found that as storms develop there tends to be a focusing of the directional energy as the peak of the storm is approached followed by directional defocusing as it decays. The effect of this upon the normalised crest elevations has been studied and sample distributions of crest heights taken from the growth, peak and decay of storms show some differences that are discussed in Wolfram and Venugopal (2003). The present paper reports the directional wave spreading and its effect upon the particle kinematics field.

The paper includes a brief description of North Alwyn MetOcean environmental monitoring station, the instrumentation installed and the data collection system. The results from the analysis of directional wave data collected during storms for the years

1994–2000 are then presented. These include the directional wave spectra, spreading functions and wave spreading factors. The paper also describes studies undertaken in the multi-directional wave basin at Heriot-watt University. Included are the descriptions of the wave basin facilities, experimental arrangements in the basin and wave particle measurements. The significance of the results is then discussed.

2. The North Alwyn MetOcean station and data collection

The North Alwyn platform is situated in the northern North Sea, about 100 mile east of the Shetland Islands (60°48.5′ North and 1°44.17′ East) in a water depth of approximately 130 m. There are two platforms (A and B) in close proximity connected by a walkway, North Alwyn 'A' being the site of all the sensor and logging equipment. Heriot-Watt University has collected wave heights, wind speed and wind directions via the sensors listed in Table 1. Fig. 1 shows the positioning of the measuring devices on the platform and the orientation of the wave altimeter triangle in earth axes. There are three Thorn EMI infra-red wave height meters in place forming a triangle with sides of approximately 51, 50 and 72.5 m. Their heights are nominally 34.33, 30.30 and 24.69 m above platform datum. Within the valid range of measurement for each of the sensors the resolution is 5 cm to an accuracy of $\pm 1\%$. During storms, the sensors may experience drop-out due to spurious reflections from spray, or other interference, in the signal path between the emitter, the water surface and the detector. In these circumstances the signal returned by the sensor is held at the last (apparently) valid datum so that any significant interval of drop-out manifests as an obvious horizontal plateau in the record.

A PC on the platform controls the data acquisition, preliminary processing of the data and local storage of the data. The central processor acquires data at 5 Hz, via a Labtech Notebook/XE software package, and creates raw data files. Readings are split into 20-min blocks for statistical treatment. The parameters calculated and stored are listed in Table 1 along with the thresholds, which enable characterisation of each block as either

Table 1
Measurement devices

Measurement	Sensor type	Statistics	Thresh-old
1. Wave height H (Marex monitor)	Thorn EMI infra-red laser wave height meter #1	Significant wave height H_{m0}	3.5 (m)
2. Wave height H (Walkway monitor)	Thorn EMI infra-red laser wave height meter #2	Significant wave height H_{m0}	3.5 (m)
3. Wave height H (North-East corner monitor)	Thorn EMI infra-red laser wave height meter #3	Significant wave height H_{m0}	3.5 (m)
Wind speed U	Munro IM 146 anemometer	Mean wind speed	16 (m/s)
Wind direction θ	Munro IM 146 anemometer	Mean wind vector w.r.t True North	–

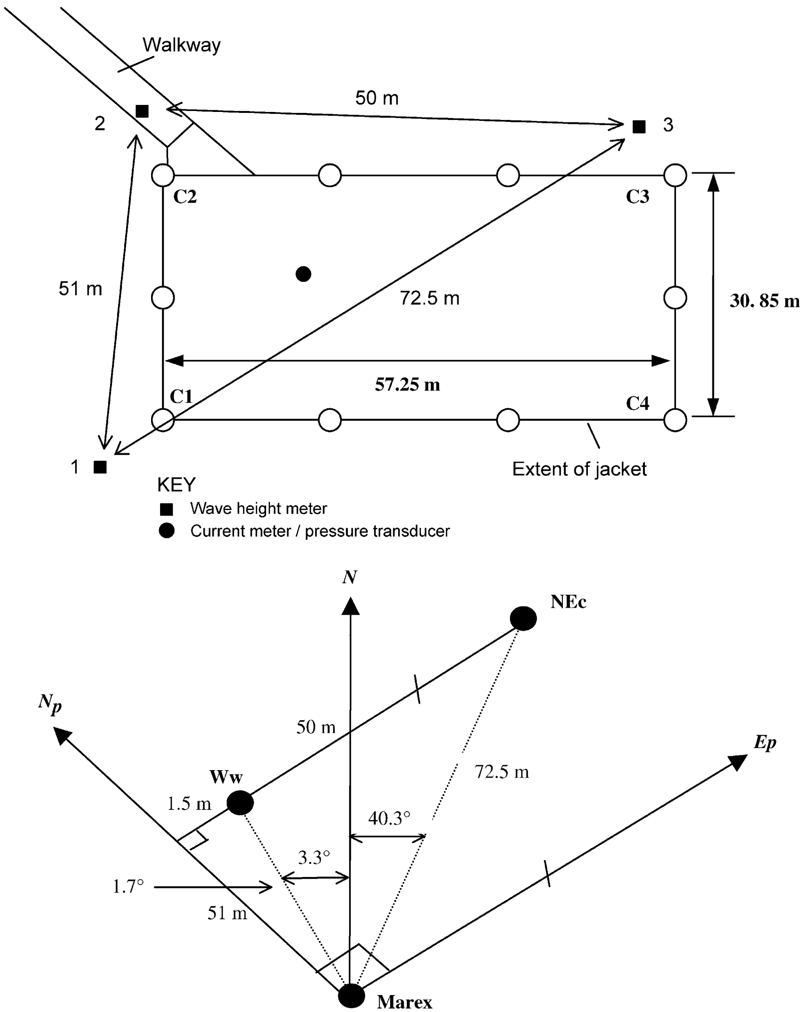

Fig. 1. Sensors positions on North Alwyn platform 'A': general layout (top) and angles between the three wave monitors (bottom).

'calm' or 'storm'. The latter is defined as a 20-min period where either of the thresholds is exceeded. The wave and wind thresholds are such that probability of exceedance is approximately 25%. When the 'storm' threshold is exceeded then all the time series data are stored for transmission back to Heriot-Watt University. When the thresholds are not exceeded then summary statistics only are calculated and retained for later transmission. The data have been transmitted to Heriot-Watt University on a daily basis, since 1994 creating the largest, continuously recorded set of Metocean data on the UK continental shelf. The storms analysed for this paper are described in Section 3.

3. Storm data analysis

3.1. Directional wave spectra and wave spreading

There are several methods for analysing directional wave data and presenting the results (Benoit and Goasguen, 1999). The maximum likelihood method of directional resolution has proved to provide reliable estimates (Isobe et al., 1984) of the directional spreading with rather a short CPU time without special tuning (Massel and Brinkman, 1998) and in the present work the *iterative maximum likelihood method* (Krogstad, 1988; Benoit et al., 1997) is used for the storm data analysis to determine the amount of sea spreading and the wave directions at the peak of the energy spectra. The directional spectrum $S(\omega,\theta)$ is expressed as the product of a directional spreading function, $D(\omega,\theta)$, and a unidirectional wave energy spectrum, $S(\omega)$, such that

$$S(\omega, \theta) = D(\omega, \theta)\, S(\omega) \tag{1}$$

where $S(\omega)$ is the frequency spectrum; $D(\omega,\theta)$, the directional spreading function with $\int_0^{2\pi} \int_0^{\infty} D(\omega, \theta)\mathrm{d}\omega\, \mathrm{d}\theta = 1$.

The wave energy at a point has an angular distribution as well as a distribution over a range of frequencies. This angular distribution of wave energy is described by the directional spreading function, $D(\omega,\theta)$. Spectral representations, $S(\omega,\theta)$ that include both the frequency distribution and the angular spreading of wave energy are known as directional spectra. In the present data analysis both the directional energy spectra and spreading functions for the storms are calculated and presented here.

Ten storms, having significant wave height from 3 to 10 m, have been chosen for detailed directional wave analysis, however, comprehensive results are reported only for Storms 95, 121 and 223 due to space limitations; details of these storms are given in Table 2. The selection of the storms was based on two criteria; (i) all three monitors were recording the waves continuously throughout the storm duration and provide records that are more consistent than those in other storms in the same year, and (ii) all these storms have a significant wave height more than 6 m. Note that there are many storms with significant wave height more than 6 m, but unfortunately one or two of the wave

Table 2
Storm details

Storm no.	Month and year	Duration (h)	Max significant wave height (m)
2	Sep, 1994	37	8.4
35	Feb, 1995	79	6.4
95	Sep, 1996	23	7.1
103	Oct, 1996	22	7.1
113	Dec, 1996	27	6.9
120	Feb, 1997	82	7.9
121	Feb, 1997	93	8.6
127	Feb, 1997	33	9.1
160	Feb, 1998	115	10.0
223	Dec, 1999	67	7.2

recordings have been affected by significant intervals of spray drop-out or wave reflection/ diffraction by the Alwyn platforms and so they have not been subjected to detailed analysis, as the wave directional analysis program requires a minimum of three good wave records. For the storms reported here, all three monitors were observed to provide almost the same wave heights (and wave height statistics) throughout the storm period.

The directional spectra for the three storms are shown in Figs. 2–4, respectively, and were obtained using the iterative maximum likelihood method. For each storm, three directional spectral polar plots are shown corresponding to (a) start of the storm, (b) close to the peak of the storm and (c) end of the storm. The wave directions in these plots are those towards which the waves are travelling; where 0 and 90° correspond to the east and north directions, respectively. The dotted concentric circle represents the frequency intervals. These plots indicate that close to the peak of the storm the wave energy is more directionally focused about a single direction. This characteristic has been observed in most storms that we have analysed using the North Alwyn data. One exception to this is Storm 121 (Fig. 3) which has a clear bimodal nature with significant energy centred around the directions of 50 and 300° at the peak of the storm.

The temporal progression of the frequency spectrum and directional spreading function for two storms (Storm 95 and Storm 121) are shown in Fig. 5(a) and (b), respectively, at different intervals of time after the start of the storm. In each case (except as noted for Storm 121) as the storm grows to its peak intensity, the spectral energy increases and energy becomes more concentrated around a single spectral peak. The spectrum showing largest density corresponds approximately to the peak of the storm. The peak spectral frequency is seen to shift towards the lower frequencies as the storm intensity increases. The spreading functions indicate a consistent trend with spectral energy. At lower spectral energies, the magnitudes of the peak spreading function are observed to be low with the energy quite spread. As the storm grows the energy becomes concentrated around the mean wave direction and spreading function has a more pronounced and larger peak.

3.2. Spreading parameter

The directional spreading function represents the directional distribution of wave energy and is known to vary with frequency. It indicates how a given energy density at each frequency is spread over the directional angle. The common forms of the directional spreading functions are: cos-2*s* distribution (Longuet-Higgins et al., 1963; Mitsuyasu et al., 1975; Hasselmann et al., 1980); *wrapped normal* distribution (Borgman, 1969; Briggs et al., 1995); *sech-2* distribution (Donelan et al., 1985); *von Mises* distribution (Hashimoto and Konube, 1986) and *Poisson* distribution (Lygre and Krogstad, 1986). Krogstad and Barstow (1999) analysed wave data collected in the WADIC, WAVEMOD and SCAWVEX projects and concluded that the general distributional shapes are between cos-2*s* and *Poisson* distributions.

The directional spreading function usually used in engineering calculations in Europe (Tucker, 1996) is of the form

$$D(\omega,\theta) = A\cos^{2s}\frac{1}{2}(\theta-\theta_0),\quad s>0,\quad 0<\theta\leq 2\pi,\quad 0\leq\theta_0<2\pi \tag{2}$$

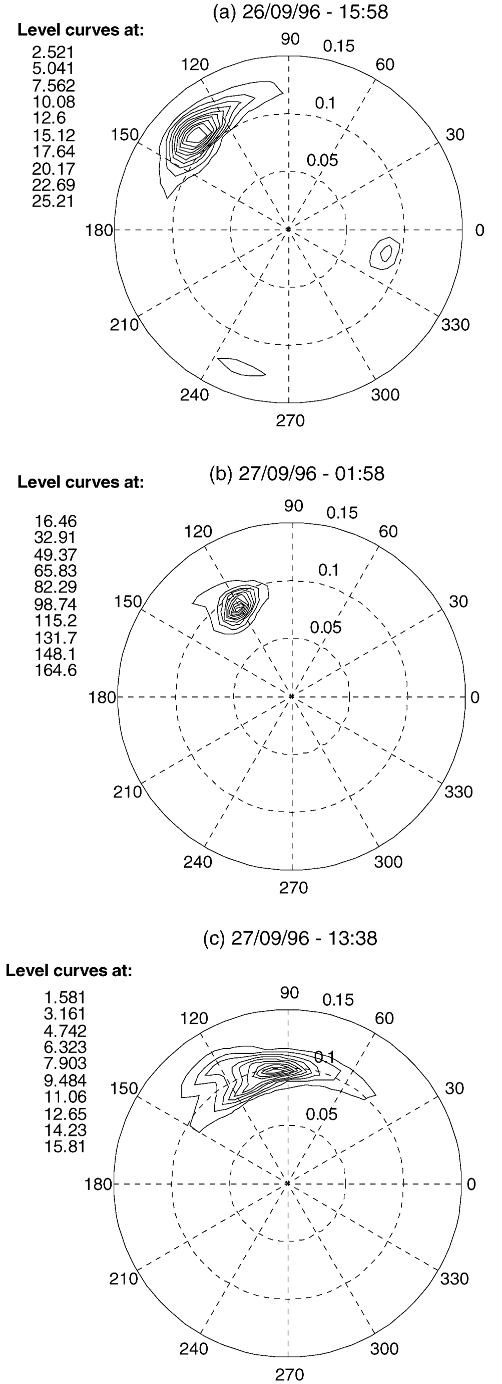

Fig. 2. Directional spectra for Storm 95: (a) start of the storm, (b) peak of the storm and (c) end of the storm.

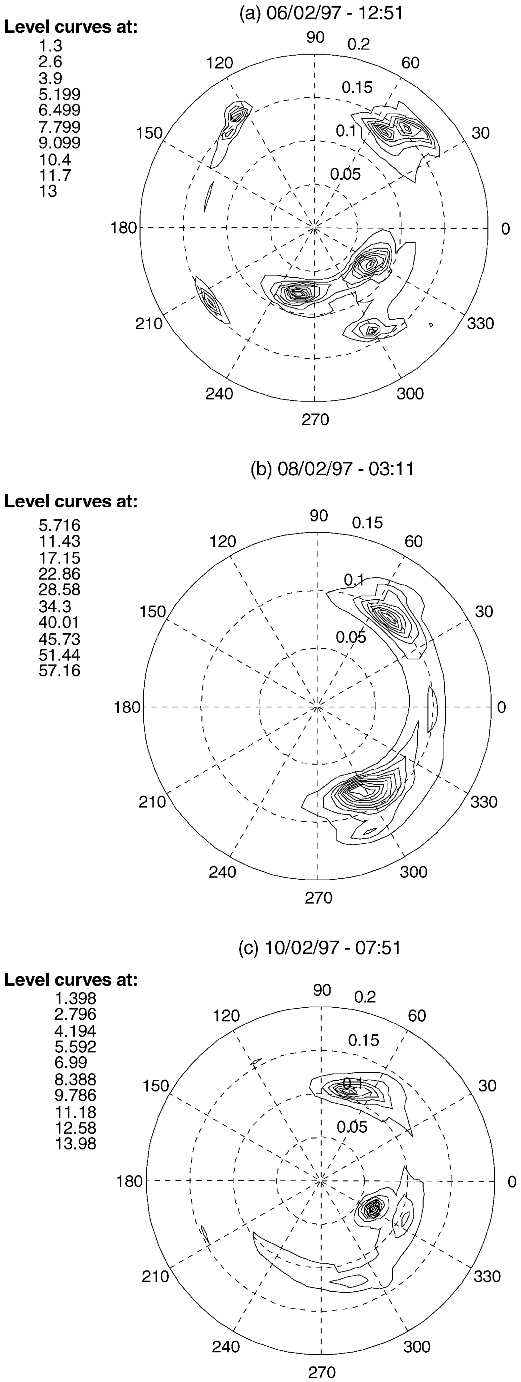

Fig. 3. Directional spectra for Storm 121: (a) start of the storm, (b) peak of the storm and (c) end of the storm.

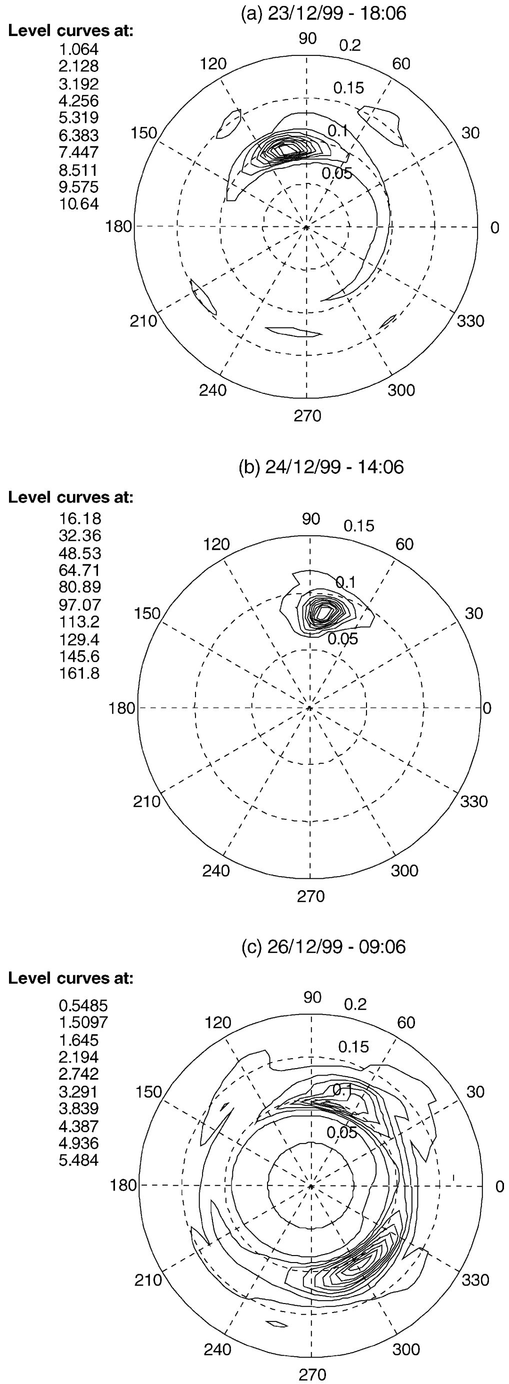

Fig. 4. Directional spectra for Storm 223: (a) start of the storm, (b) peak of the storm and (c) end of the storm.

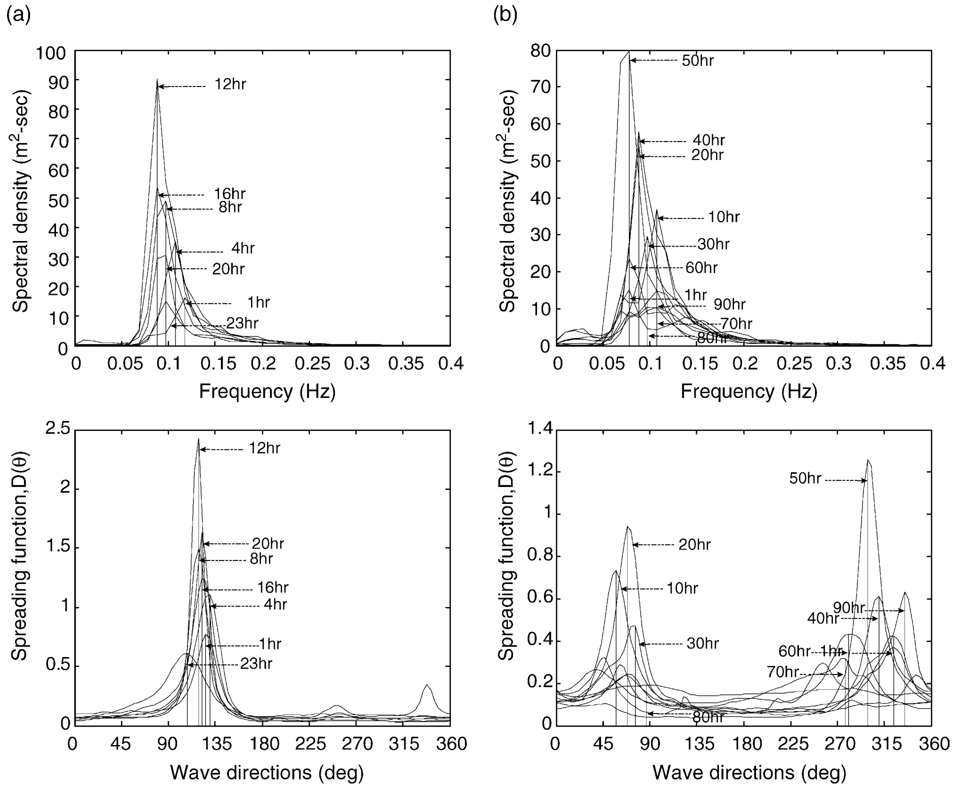

Fig. 5. Energy spectrum (top) and spreading function (bottom): (a) Storm 95 and (b) Storm 121.

where

$$A = \frac{2^{2s-1}}{\pi} \frac{\Gamma^2(s+1)}{\Gamma(2s+1)} \tag{3}$$

$\Gamma(\cdot)$ indicates the Gamma function and s is a function of the wave frequency which controls the concentration of the directional distribution of the wave energy and θ_0 is the mean wave direction. The spreading parameter s can be calculated from the Fourier coefficients of the measured spreading functions by expressing it as a Fourier series (see Tucker (1991) for details)

$$D(\omega, \theta) = \frac{1}{2\pi}\left[1 + 2\sum_{n=1}^{\infty}\{r_n(\omega)\cos(n(\theta - \theta_n(\omega)))\}\right] \tag{4}$$

Fig. 6 shows the relationship between significant wave height, H_S and the spreading parameter s and these value calculated for the ten storms listed in Table 2. Each point represents the spreading parameter for a 20-min wave record. Many of the larger values of spreading indices correspond to higher significant wave heights, which indicate that during the storm peaks the waves tend to become less spread.

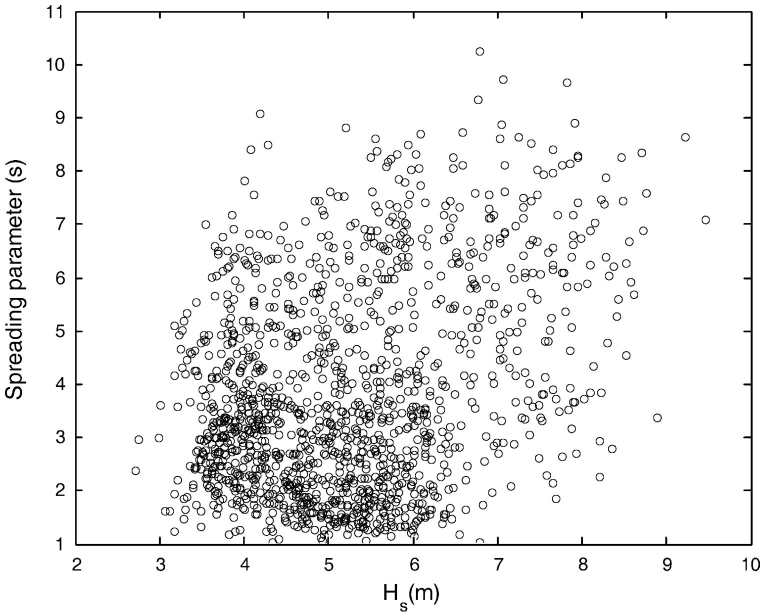

Fig. 6. Significant wave height vs spreading parameter (s).

3.3. Wave kinematics factor (or wave spreading factor) from field data

The report by Tucker (1996) provides details of the definition of the wave kinematics factor (F_S). The wave kinematics factor is also known as the wave spreading factor in this report. Wave measurements from eight stations around the UK have been used in this report and the values of the kinematics factor obtained are discussed. According to Tucker (1996), the definition of F_S is *the factor by which the root mean square amplitude of the component of the wave orbital velocity which is in-line with the mean wave direction is reduced relative to what it would be for a unidirectional wave system with the same point spectrum*. Two definitions of kinematics factor were given by Tucker (1996); F_{S1}, and F_{S2} derived from first and second angular harmonics of the directional wave spectrum and expressed as a function of frequency, ω

$$F_{S1}(\omega) = C_1(\omega) \tag{5}$$

$$F_{S2}(\omega) = \left[\frac{1}{2} + \frac{1}{2}C_2(\omega)\right]^{1/2} \tag{6}$$

where $C_1(\omega)$ and $C_2(\omega)$ are the amplitude of the first and second angular harmonics. Tucker indicates that for most practical purposes the value of the wave kinematics factor at the peak of the spectrum, $F_{S2}(peak)$, is specified as this is conservative as the angular beamwidth of a wave system is narrowest close to the spectral peak. On the assumption that the wave spreading function follows a cos-2s distribution, the wave kinematics factor

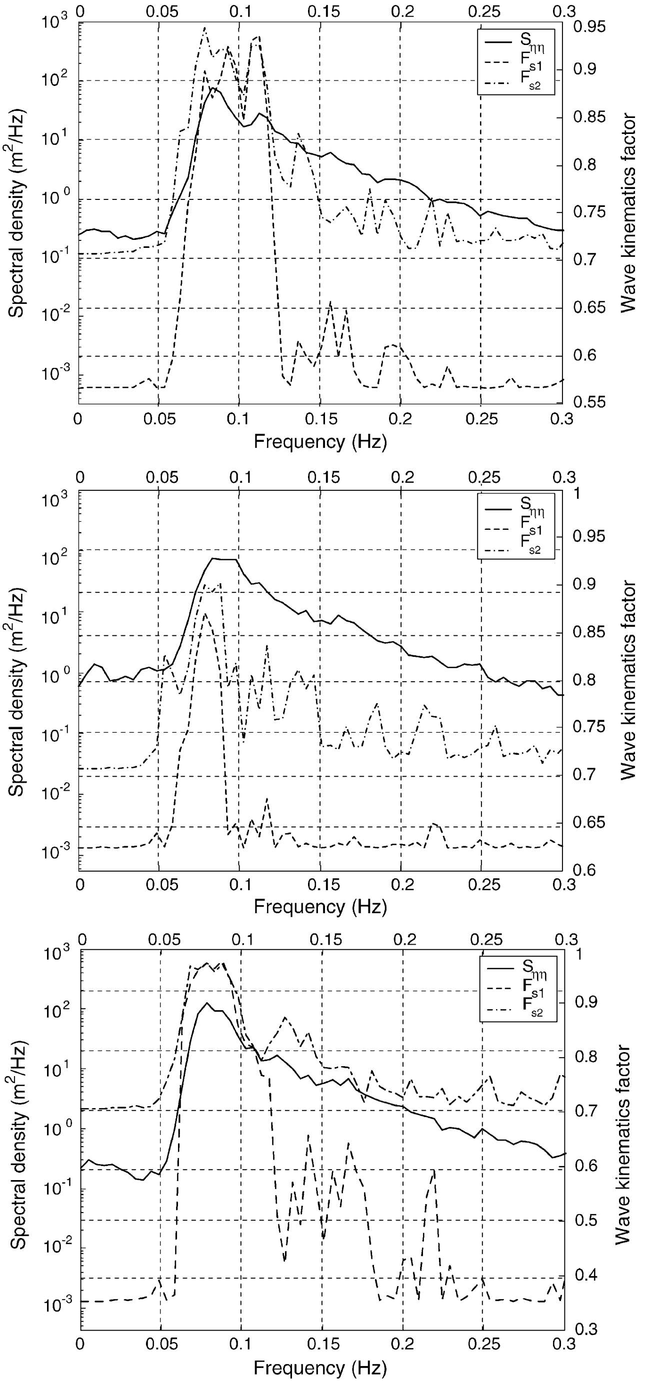

Fig. 7. Wave spreading factors with frequency; Storm 95 (top), Storm 121 (middle) and Storm 223 (bottom).

can also be written as

$$F_{S1}(\omega) = \frac{s}{s+1} \tag{7}$$

$$F_{S2}(\omega) = \left[\frac{s^2+s+1}{(s+1)(s+2)}\right]^{1/2} \tag{8}$$

where s the spreading parameter calculated as a function of ω from first and second angular harmonics for F_{S1} and F_{S2}, respectively. These two factors are plotted in Fig. 7 for Storms 95, 121 and 223. These plots correspond to 20 min wave records picked up from the peak of each storm. Note that for the purpose of clarity the frequency axis is shown only up to 0.3 Hz, however, the whole spectrum has been included in the computations wherever necessary. Fig. 7 clearly demonstrates the difference between the definitions, F_{S1} and F_{S2}. The theoretical minimum values of F_{S1} and F_{S2} are 0.0 and $1/\sqrt{2}$, respectively, for an isotropic sea (Tucker, 1996), and this is reflected in these figures; around the peak of the spectrum, these two values are closer. Tucker (1996) reported that F_{S2} is the best parameter for engineering use because for any beamwidth, the factor F_{s2} is a correct measure of the root-mean-square (rms) in-line velocity as a proportion of the total rms velocity. Three different definitions of wave kinematics factor adopted from Tucker (1996) are used here:

(i) $F_S(peak)_1$—computed from the single spectral estimate at the frequency corresponding to the measured spectral peak;
(ii) $F_S(peak)_3$—computed from the average over three spectral estimates centred on the measured spectral peak; and
(iii) $F_S(mean)$—computed as the energy-weighted spectral mean.

These three values are tabulated in Table 3 for three storms and the kinematics factor are those corresponding to the still water level ($z=0.0$ m).

The spreading factor can also be expressed as [ISO/TC67/SC7/WG3, ISO/CD 19901-1 (draft), 2002, in Annex-A.7.6]

$$\phi^2 = 0.5\left[1+\frac{s(s-1)}{(s+1)(s+2)}\right] \tag{9}$$

Note that Eq. (9) is same as Eq. (8) and gives the same result for a given value of s. Using spectrally weighted averaged values of the spreading parameter, s (frequency

Table 3
Wave kinematics factor computed based on the definitions by Tucker (1996)

Storm no.	F_{s1} $(peak)_1$	F_{s1} $(peak)_3$	F_{s1} $(mean)$	F_{s2} $(peak)_1$	F_{s2} $(peak)_3$	F_{s2} $(mean)$
95	0.8714	0.8871	0.8087	0.9127	0.9265	0.8662
121	0.8535	0.8441	0.6619	0.8933	0.8983	0.7838
223	0.9745	0.9662	0.8692	0.9747	0.9653	0.912

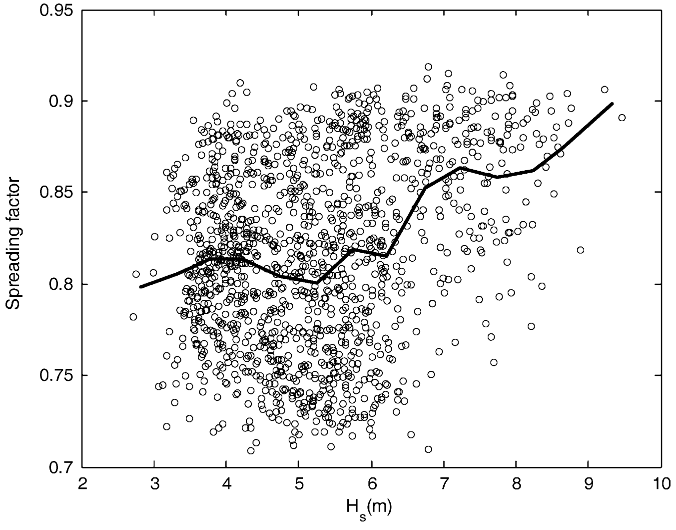

Fig. 8. Significant wave height vs spreading factor (ϕ).

independent), the spreading factors have been calculated and are plotted in Fig. 8 against the significant wave height. Each data point represents the value calculated from a 20 min wave record.

4. Experiments in the wave basin

4.1. Equipments and instrumentation

The experiment programme, carried out in the multidirectional wave basin of the Department of Civil and Offshore Engineering, Heriot-Watt University, aimed to reproduce extreme storm waves in the basin to measure the wave kinematics in long and short-crested waves with different spreading indices. The measured wave kinematics were then compared with theoretical wave kinematics using linear and second order hybrid wave models (Zhang et al., 1999).

The dimensions of the wave basin are 12 m $\times$ 12.4 m with a working water depth of 3 m and a deep pit of 5 m in depth. The basin is equipped with a wave making system of electro-mechanical flap-type wave makers across the width of the tank at one end. The wave generators are capable of producing unidirectional regular and random waves and random steep short-crested waves up to 0.5 m high. At the other end of the tank there is a parabolic mesh beach that effectively dissipates most of the wave energy. There are 24 wave paddles in the wave making system, each paddle is 0.5 m wide and is independently controlled so that both long-crested and short-crested waves can be produced. The wave maker can generate regular and random waves in the frequency range of 0.2–2.5 Hz.

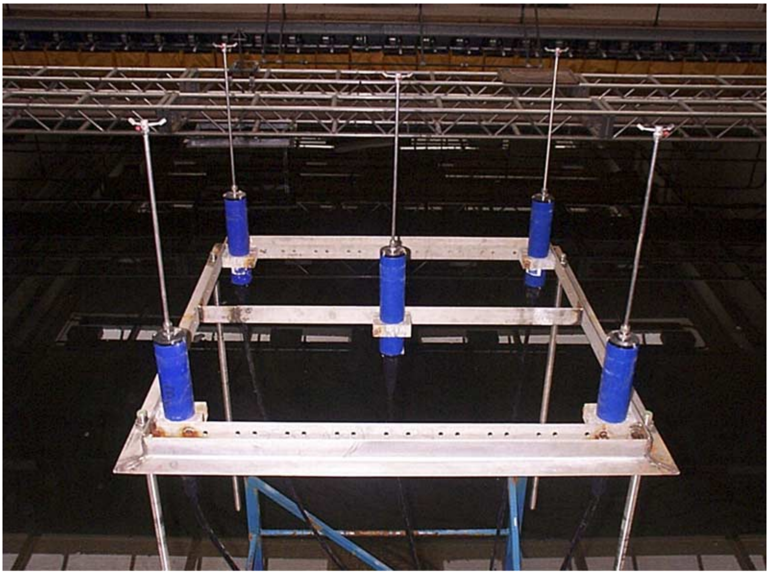

Photo 1. Current meters mounted onto the experimental rig for wave kinematics measurements.

A computer drives the paddles using the *Ocean* software developed and installed by Edinburgh Designs (Rogers and King, 1997).

An experiment rig (Photo 1) was designed and built to support the wave particle velocity meters so that measurements of the particle kinematics could be made below the waves on a horizontal grid at different depths. This horizontal grid could be raised and lowered to make measurements at different heights allowing a 3-D array of point measurements during a series of repeat experiments. In essence the rig comprises two horizontal square frames. The lower frame is fixed to the bottom of the basin; adjustable legs attach the upper frame to it so that the elevation of the upper frame can be adjusted between experimental runs. Five detachable aluminium blocks, each with a central hole for fixing the current meters, are fixed to the top frame, one at the centre of the frame and other four blocks at four corners of the top square frame. The blocks can be moved in the horizontal plane on the upper frame to any desired location to allow a variety of measurement configurations. The current meters are fixed in the holes in an inverted position so that the body of the devices are below the measuring heads and all the connecting cables are far away from the measuring region to ensure that the measurements will be as free from disturbances as possible. The rig has an overall height of about 2 m and is made from steel sections with considerable cross bracing to ensure it remains rigid during the experiments.

Another aluminium frame with the same plan dimensions as the top frame of the experiment rig has been fabricated, onto which six wave probes (P1, P2, P3, P4, P5 and P6) are fixed as shown schematically in Fig. 9. The wave probes are placed directly above the current meters to avoid any phase delay between the wave and velocity records.

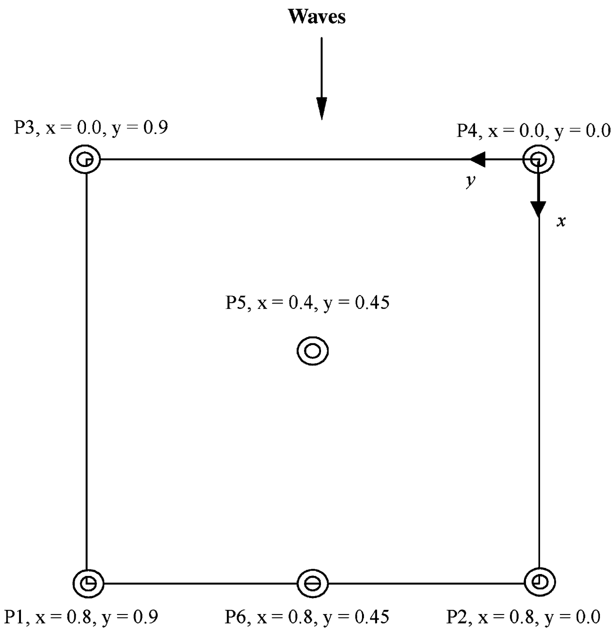

Fig. 9. Schematics arrangement of square array.

Five NDV Velocimeters (Nortek As, 2000) were used in the experiments to measure the wave particle kinematics. The PC-based NDVLab velocimeter (Photo 1), comprises (i) three acoustic receivers and a transmitter mounted on a rigid 40 cm stem, (ii) an end-bell and (iii) a cable of 20 m to connect to the PC. The velocity is measured in three directions at a sampling rate of 25 Hz to an accuracy of $\pm 1\%$. The analogue output channel of each ADV card was used so that data from all the wave height probes and the current meters could be collected on a common time base. Data from the wave probes and current meters was sampled by a Data Translation CIO-DAS6402/16 64-Channel 100 KHz, 16 bit, ADC using LabVIEW 4.1. The water in the basin was seeded with hollow glass spheres (Trade name: Spherical-110P8, manufactured by Potters Industries, Inc., Southpoint, USA) to ensure proper functioning of the velocimeters during measurements.

4.2. Storm waves reproduction

Storms 95, 121 and 223 were selected for reproduction in the basin using the *Ocean* wave software. A scale of 1:55 was chosen to satisfy as closely as possible the constraints imposed by the tank depth, clock-frequency and run number to match the full-scale water depth of 130 m, plus tide, at North Alwyn; this choice of scale gave a corresponding depth of 159 m. For each storm a 3-h wave elevation time history from the peak of the storm, corresponding to one monitor record, was scaled down in height and frequency. A 5% lead-in and a 10% roll-off was applied at the start and end of each record, respectively,

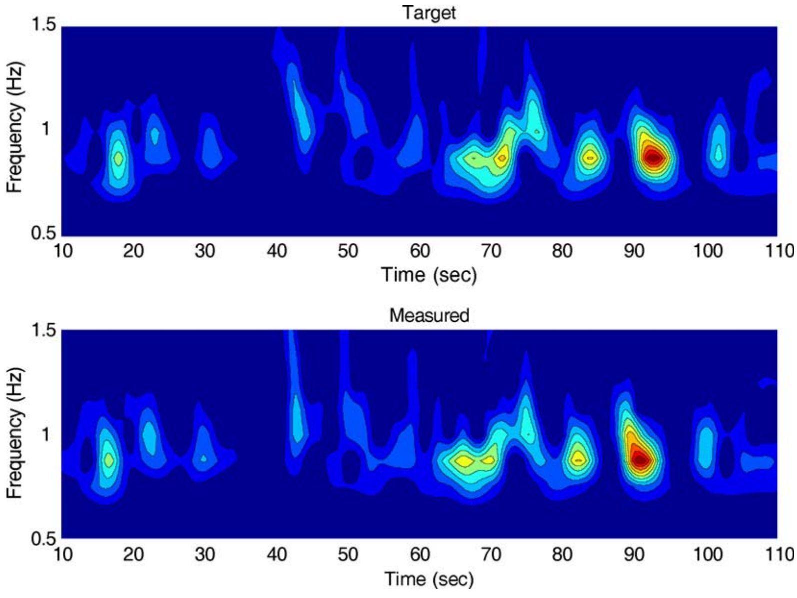

Fig. 10. Comparison of measured and target time–frequency plots obtained using S-Transform method.

using a Hanning window to limit starting and stopping transient waves and consequent damage to the wave paddles. Fig. 10 shows a typical comparison of time–frequency contour plots of wave energy, obtained using the Stockwell transform (S-transform) (Stockwell et al., 1996; Linfoot et al., 2000), for a portion of the measured and target records. It is evident that the wave groups on the measured times series occur at similar locations on the time–frequency plane as those of the target record. A slight difference in the energy contours at lower energy levels may be ignored when one is interested in extreme waves. The *Ocean* software package allows only the cos-2s form of directional spreading and hence this spreading function was applied to the unidirectional waves with spreading indices $s=2$, $s=4$, $s=8$ and $s=\infty$. Each of the 3-h storm records was reproduced in the basin with these four spreading indices so that the same wave elevation record (and hence the same spectral energy) was used as input for both unidirectional and multidirectional waves.

4.3. Wave kinematics measurements in the wave basin

The wave kinematics were measured at depths $z=0.20$, 0.35 and 0.50 m below the still water level, corresponding to depth of 11, 19.25 and 27.5 m, respectively, at full-scale. The wave particle velocities in three perpendicular (x, y and z) directions, V_x, V_y and V_z and the wave elevations from each probe were recorded simultaneously with a sampling frequency of 25 Hz.

Using the measured particle kinematics it is possible to directly obtain the wave kinematics reduction factor for short-crested seas. The kinematics reduction factor, F_S can be calculated using the following expression (Tucker, 1996)

$$F_s = \sqrt{\frac{\sigma_u^2}{\sigma_u^2 + \sigma_v^2}} \tag{10}$$

where σ_u and σ_v are the root mean square values of horizontal velocities V_x and V_y, respectively. In the case of a directional sea these are the velocity components in-line and perpendicular to the mean wave direction.

Since the particle kinematics were measured at three different depths below the still water level, we have examined the effect of varying the depth of measurement on the kinematics reduction factor. The calculations of F_s have been carried out for three storms and are given in Tables 4–6. The current meter at probe P3 was excluded from the analysis as the recordings from this particular instrument were frequently corrupted by severe noise. The mean of the depth-averaged values ($=\sum_{n=1}^{4} wp_n$, n is the number of probe) and their standard deviations for each spreading parameter were calculated and are shown in Table 7.

The spreading factor (F_S) values in Tables 4–6 computed using the measured velocities in both the horizontal directions indicate that the kinematics reduction factor does not show any significant variation with respect to changes of measurement depth for all four velocity probes and for all three storms. However, these values indicate that particularly when the sea is wide spread (i.e. for smaller spreading parameter, s), F_S could be different with respect to measurement locations in the horizontal plane, as there exists a considerable variation between the four velocity probes. The depth-averaged spreading factor given in Table 7 reveals that F_S increases with increased spreading parameter irrespective of the wave characteristics. Theoretically a constant value of $F_S = 1.0$ is expected for all unidirectional waves ($s = \infty$). In our experiments, values in the range of 0.985–0.992 were obtained. The lower range of $F_S = 0.985$ may indicate the existence of a transverse velocity component (perpendicular to the main wave direction) in the wave basin or due to one of the reasons discussed in Section 5.

5. Second order wave kinematics calculation

The hybrid wave model (Zhang et al., 1996, 1999) has been used to calculate the wave particle kinematics of the storms measured at the platform, as no direct measurements of velocity were available during these storms. The predictions of particle kinematics were used to estimate the wave kinematics factor and these were then compared with the factors obtained through the experiments in the wave basin.

The hybrid wave model has the capability of predicting short distance wave evolution and kinematics in directional seas and its accuracy in the prediction of wave properties of nonlinear waves has been validated in many publications. It requires time series from a minimum of three wave properties as input; one of the inputs should be a wave surface elevation or a pressure measurement record and others can be horizontal velocity components. The model includes the effects of the nonlinear interaction among wave components and is correct up to second order wave steepness. The algorithm consists of

Table 4
Kinematics factor (F_s) for Storm 95 calculated from wave basin measurements

Depth of measurements	$s=2$				$s=4$				$s=8$				$s=\infty$			
	wp1	wp2	wp4	wp5	wp1	wp2	wp4	wp5	wp1	wp2	wp4	wp5	wp1	wp2	wp4	wp5
−0.20 m	0.719	0.738	0.769	0.764	0.829	0.819	0.794	0.866	0.914	0.901	0.904	0.911	0.991	0.989	0.989	0.993
−0.35 m	0.706	0.739	0.762	0.766	0.816	0.835	0.852	0.86	0.924	0.907	0.906	0.916	0.989	0.989	0.984	0.989
−0.50 m	0.712	0.718	0.773	0.751	0.811	0.8	0.819	0.834	0.917	0.891	0.901	0.903	0.973	0.987	0.977	0.977
Mean (depth averaged-values)	0.712	0.732	0.768	0.76	0.819	0.818	0.822	0.853	0.918	0.9	0.904	0.91	0.984	0.988	0.983	0.986
Std deviation	0.0065	0.0118	0.0056	0.0081	0.0093	0.0175	0.0291	0.017	0.0051	0.0081	0.0025	0.0066	0.0099	0.0012	0.006	0.0083

Table 5
Kinematics factor (F_s) for Storm 121 calculated from wave basin measurements

Depth of measurements	$s=2$				$s=4$				$s=8$				$s=\infty$			
	wp1	wp2	wp4	wp5	wp1	wp2	wp4	wp5	wp1	wp2	wp4	wp5	wp1	wp2	wp4	wp5
−0.20 m	0.726	0.761	0.766	0.759	0.831	0.856	0.866	0.861	0.929	0.914	0.911	0.921	0.992	0.99	0.989	0.993
−0.35 m	0.723	0.773	0.774	0.764	0.84	0.855	0.866	0.872	0.933	0.924	0.918	0.929	0.995	0.993	0.991	0.995
−0.50 m	0.714	0.758	0.779	0.763	0.825	0.85	0.858	0.85	0.925	0.911	0.909	0.916	0.991	0.988	0.987	0.993
Mean (depth-averaged values)	0.721	0.764	0.773	0.762	0.832	0.854	0.863	0.861	0.929	0.916	0.913	0.922	0.993	0.991	0.989	0.994
Std deviation	0.0062	0.0079	0.0066	0.0026	0.0075	0.0032	0.0046	0.011	0.004	0.0068	0.0047	0.0066	0.0021	0.0025	0.002	0.0012

Table 6
Kinematics factor (F_s) for Storm 223 calculated from wave basin measurements

Depth of measurements	$s=2$				$s=4$				$s=8$				$s=\infty$			
	wp1	wp2	wp4	wp5	wp1	wp2	wp4	wp5	wp1	wp2	wp4	wp5	wp1	wp2	wp4	wp5
−0.20 m	0.735	0.746	0.753	0.737	0.84	0.845	0.865	0.859	0.921	0.905	0.908	0.911	0.992	0.989	0.988	0.993
−0.35 m	0.731	0.752	0.756	0.747	0.844	0.851	0.861	0.865	0.928	0.918	0.915	0.923	0.988	0.988	0.984	0.99
−0.50 m	0.717	0.735	0.747	0.732	0.826	0.835	0.857	0.843	0.915	0.898	0.9	0.902	0.99	0.988	0.988	0.993
Mean (depth-averaged values)	0.728	0.744	0.752	0.739	0.837	0.844	0.861	0.856	0.921	0.907	0.908	0.912	0.99	0.988	0.987	0.992
Std deviation	0.0095	0.0086	0.0046	0.0076	0.0095	0.0081	0.004	0.0114	0.0065	0.0101	0.0075	0.0105	0.002	0.0006	0.0023	0.0017

Table 7
Kinematics factors calculated for wave basin measurements; mean of the depth-averaged values and standard deviation values in brackets

Spreading parameter (s)	Storm 95	Storm 121	Storm 223
2	0.743 (0.026)	0.755 (0.023)	0.741 (0.010)
4	0.828 (0.017)	0.853 (0.014)	0.849 (0.011)
8	0.908 (0.008)	0.920 (0.007)	0.912 (0.006)
∞	0.985 (0.003)	0.992 (0.002)	0.989 (0.002)

Note: Exaggerated for clarity. Np and Ep are platform north and platform east.

two parts: (i) decomposition of a wave time series which decouples the nonlinear contributions from the time series so as to effectively separate the free-wave and bound-wave components; (ii) superposition of wave time series to compute the nonlinear contributions to any wave property and then the superposition of these on to those computed from the free-wave components. The decomposition part produces free-wave amplitudes, phases and wave directions for the range of frequency considered. The interaction of two-wave components is modelled in the hybrid wave model by using both the conventional mode coupling (MCM) solution (Longuet-Higgins and Stewart, 1960) and the phase modulation method (PMM) (Zhang and Melville, 1990). The PMM is a complementary solution to the divergence of the MCM because the MCM may not converge if the wavelengths of the two interacting wave components are quite different. Unlike linear wave theory and its various empirical and semi-empirical modifications, the hybrid wave model is valid for finite amplitude waves. It satisfies the continuity equation governing wave-induced fluid kinematics up to the free surface, and up to the second-order in wave steepness.

The hybrid wave model was used to investigate the spatial variation of wave crest heights and the particle kinematics field within an area occupied by the North Alwyn platform. In particular, the wave surface elevation and wave particle kinematics were predicted at the locations of the four main columns (C1, C2, C3 and C4) (c.f. Fig. 1) [C1 ($x=9.3$; $y=9.3$ m), C2 ($x=5.2$; $y=39.8$ m), C3 ($x=62.4$; $y=46.13$ m) and C4 ($x=66.5$; $y=15.25$ m)]. For this purpose a 20 min wave record from the three wave altimeters at the peak of each storm was used as input for the decomposition part of the directional hybrid wave model. The kinematics reduction factors were derived using Eq. (10). A typical comparison of the measured and recovered (predicted) wave elevation time histories at the Marex and North-East corner monitors are shown in Fig. 11, for a portion of the 20 min record for Storm 121. This shows a satisfactory correlation between measurement and prediction as would be expected if the model decomposition procedure has been successful.

The kinematic factors obtained from the experiments and the full-scale data are put together in Fig. 12 for all the three storms. Three sets of F_S values are plotted here: (i) F_S corresponding to the wave basin results, (ii) F_{S2} (*mean*) calculated from the second angular harmonic as detailed by Tucker (1996) for the field data and (iii) F_S computed from the predicted wave kinematics of the field data using hybrid wave model. For case (iii), wave particle velocities are calculated at depths 10, 20 and 30 m below still water level, which are approximately corresponding to the measurements depths of 11, 19.25 and 27.5 m,

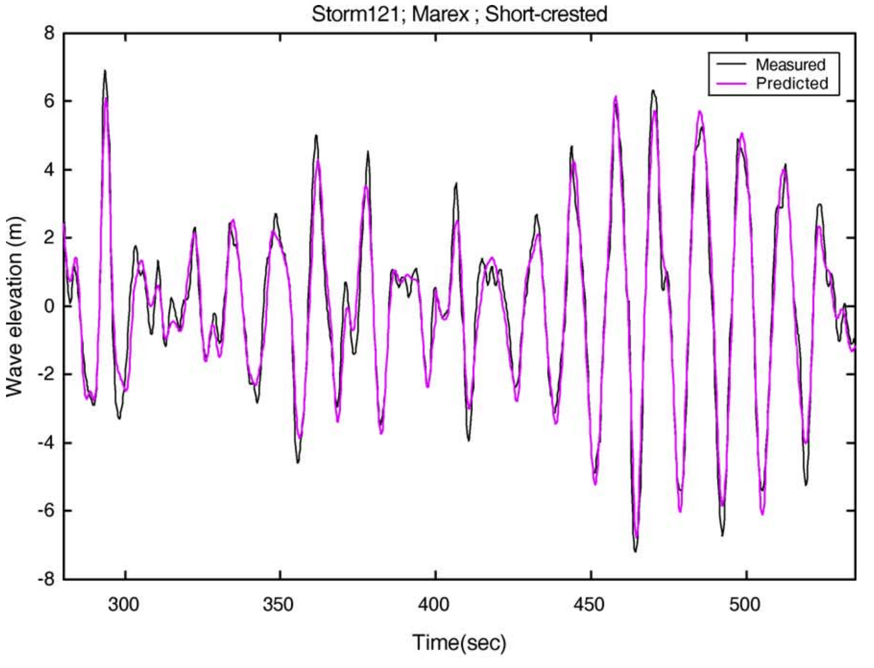

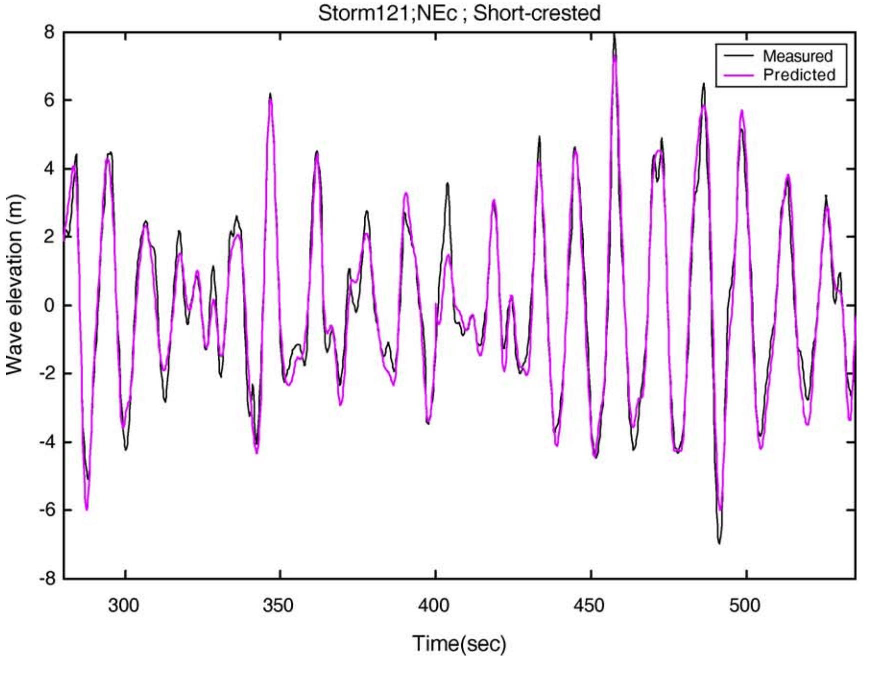

Fig. 11. Comparison between input and recovered wave elevations using hybrid wave model: (i) Marex (top) and (ii) North-East corner (bottom) monitors.

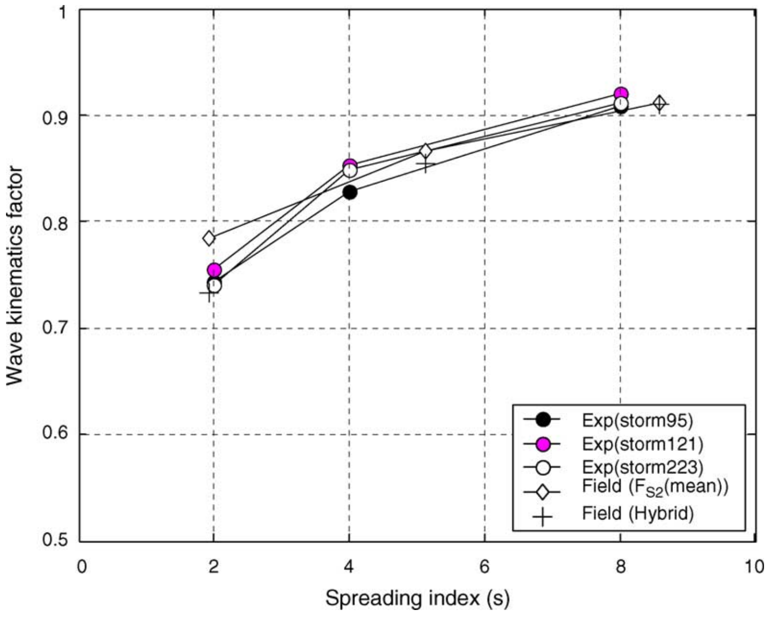

Fig. 12. Wave kinematic factors computed from field measurements and wave basin experiments.

respectively, in the wave basin. The wave kinematic factors are then obtained for all the four columns location, C1, C2, C3 and C4 and then averaged for a representative value. At lower *s* values, there exists a slight difference between F_{S2} (*mean*) and F_S computed from the hybrid wave model, even though they are calculated from the same field data set. Tucker (1996) showed that F_S calculated from Eq. (10) could be comparatively smaller than F_{S2} (*mean*) for the same data and this is seen in Fig. 12. The Storm 121 has a larger significant wave height compared to Storm 95 and Storm 121, however, the kinematics factor obtained for this storm is smaller than the other two and this could be attributed to the bi-model nature of the wave spectra. Forristall and Ewans (1998) reported that bi-modal spectra are likely to have low kinematic factors, when waves from two or more storm systems combine, as different modes have different directions of travel.

6. Discussions

The variety of ways of defining and calculating kinematics reduction factor yields a range of values from the same storm conditions. Here factors based on full-scale measurements of surface elevation are considered. Fig. 7 has plots of F_{S1} and F_{S2} for the temporal peaks of the three storms which show significant variation with frequency yielding the largest values close to the peak frequency. The six different reduction factors, using Tucker's definitions, for each storm are seen to vary significantly in Table 3. Tucker (1996) suggests that the factors $F_{s2}(peak)_3$ and $F_{s2}(mean)$ should be considered for the *UK* waters; for the two uni-modal storms considered here the corresponding values are: $F_{s2}(peak)_3=0.93$ and $F_{s2}(mean)=0.87$ for Storm 95 ($s=5.13$); and $F_{s2}(peak)_3=0.97$ and $F_{s2}(mean)=0.91$ for Storm 223 ($s=8.58$). For data collected at North Cormorant, which is less than 50 miles from North Alwyn, Tucker (1996) obtained F_{s2}values ranging from 0.87 to 0.96 at the height of severe storms with an average of 0.92. He also reported that $F_{s2}(peak)_3$ can be as high as 0.97 for some severe storms and gave typical values for extreme significant wave heights of $F_{s2}(peak)_3=0.95$ and $F_{s2}(mean)=0.90$ at moderate depths; very similar to the North Alwyn values reported here. When considering the extreme wave loading on a jacket structure, which is likely to occur due to a single large wave at or close to the spectral peak frequency, then $F_{s2}(peak)_3$ might seem appropriate. However, the ISO draft standard (ISO/TC67/SC7/WG3, ISO/CD 19901-1 (draft), 2002), in Annex-A.7.6] and all authors, it appears, other than Tucker use just $F_{s2}(mean)$ or an equivalent formulation.

At North Alwyn for any given significant wave height there is a considerable range of spreading parameter values that can occur as can be seen in Fig. 6, where s is plotted for every 20 min record for the whole duration of ten separate storms. In Fig. 8, the corresponding $F_{s2}(mean)$ is seen to vary from 0.707 (the minimum theoretical value) to 0.92 and the median value is seen to rise with H_S. This trend has also been observed by Forristall and Ewans (1998) in other data sets. These median values of $F_{s2}(mean)$ would be appropriate for fatigue calculations. On the other hand, for extreme loading on a fixed platform, where the wave length is large compared to the platform dimensions, storms with the highest spreading parameter s will produce the most severe conditions; and so extreme design condition storms need to be characterised by a spreading parameter as well as by spectral density.

Wave spreading and particle kinematic reduction factors have been found to vary with latitude and this is reflected in the new ISO draft standard. Forristall and Ewans (1998) recommended an overall median value of 0.88 (low-latitude monsoons) and a value of 0.867 (tropical cyclones) for waves over 7.0m for engineering calculations, whereas values for extra-tropical areas are somewhat higher. The draft ISO standard (which quotes Forristall and Ewans (1998)) gives an expression for F_{s2} as a function of latitude and for that of North Alwyn it is 0.89, which is very similar to the $F_{s2}(mean)$ values above.

Ideally, kinematic reduction factors should be based on the measurement of the wave particle kinematics and this has been done for the experiments in the wave basin. The kinematic reduction factors computed using the measured in Tables 4–6 show little variation with depth for all the four velocity probes and for all three storms. The depth-averaged spreading factor presented in Table 7 shows the variation between storms of the same spreading parameter is between 1 and 2%, and much smaller than the variation with spreading parameters. Theoretically a value of $F_S=1.0$ is expected for unidirectional waves ($s=\infty$); however, values in the range of 0.985–0.992 were obtained, which gives a measure of the error and bias in the experiments. Some of these may be due to measurement error, some due to slight misalignment of the rig in the wave basin and some due to currents set-up in the basin during the experiments.

Fig. 12 shows the mean of the depth-averaged kinematic reduction factors (F_S) computed using horizontal velocity estimates obtained from the hybrid second order model with the surface elevation measurements made at North Alwyn platform during the three storms. These show generally very good agreement with those obtained from the corresponding wave basin velocity measurements except at $s=1.92$. However, it must be remembered that the field data for this storm, Storm 121, is bi-modal whereas all the storms in the wave basin were given a cos-2s spreading function and so differences are to be expected in this case. The capacity of the hybrid second order model to represent the wave surface elevation is shown in Fig. 11. These results show 3-D hybrid second order model is able to predict particle kinematics from surface elevations, measured at different points in the horizontal plane, with sufficient accuracy to compare well with the measured values.

All the reduction factors in Tables 4–7 and in Fig. 12 are based directly on the variance of horizontal wave particle velocities; or theoretical estimates of this variance from the surface elevation. It would of course be possible to define a reduction factor in terms of the mean of the peak amplitudes of the velocities, or the average of the tenth highest peaks, or even the highest peaks. The question of which definition of F_S is appropriate must be considered in the context of the wave loading that is to be estimated.

In light of the above results from full-scale measurements of storm waves and the velocity measurements in the basin it seems that a kinematics reduction factor $F_{S2}(mean)$ estimated from surface elevation records, and F_S based on depth-averaged root mean horizontal wave particle velocities are the most suitable definitions for calculating forces on a jacket structure. These two definitions give comparable results and hence with reference to Fig. 12, for the northern North Sea, the wave kinematic factors, $F_s=0.78$ ($s=2$); $F_s=0.85$ ($s=4$); $F_s=0.88$; ($s=6$) and $F_s=0.92$ ($s=8$) seem appropriate.

7. Conclusions

This study has investigated some of the directional properties of storm waves in the northern North Sea using full-scale data measured at a platform and experiments in a multidirectional wave basin where these storms have been simulated. The salient findings derived from this investigation are given below

1. Wave kinematic factors estimated from (i) directional wave spectrum and spreading functions computed from the surface elevation measurements at North Alwyn and (ii) wave particle kinematics predictions using hybrid second order model, tie-in quite well with the measurements made in the wave basin.
2. Wave kinematic factors vary with the spreading parameter s and for the northern North Sea the following values are appropriate: $F_s=0.78$ ($s=2$); $F_s=0.85$ ($s=4$); $F_s=0.88$ ($s=6$) and $F_s=0.92$ ($s=8$).
3. For the assessment of fixed structures the wave kinematics factor (or wave spreading factors or kinematics reduction factor) for the peak of the storm only should be used when considering the loading for fixed structures. For floating structures more extreme conditions may arise in bi-modal storms and no explicit recommendations can be made from the work described in this paper.

Acknowledgements

The authors are grateful to Total Oil Marine for supporting the operation of the environmental monitoring station and data collection programme at North Alwyn platform and to Health and Safety Executive Offshore Safety Division, United Kingdom, for funding this research. The authors are grateful to Jun Zhang and his research group, Ocean Engineering Program, Texas A&M University, USA for the permission to use the Hybrid wave model program.

References

Aage, C., Jorgensen, P., Andersen, L.W., Dahl, C., Klinting, P., 1989. Wave loads on a cylinder in 2-D and 3-D deep water waves, Proceedings of the Eighth International Conference on Offshore Mechanics and Arctic Engineering, The Hague, March 19–23, vol. 2 1989 pp. 175–181.

API, 1993. Recommended practice for planning, designing and constructing fixed offshore structures—load and resistance factor design. American Petroleum Institute, Washington, p. 225.

Benoit, M., Goasguen, G., 1999. Comparative evaluation of directional wave analysis techniques applied to field measurements, Proceedings of the Ninth International Offshore and Polar Engineering Conference, Brest, France, May 30–June 4, vol. III 1999 pp. 87–94.

Benoit, M., Frigaard, P., Schaffer, H.A., 1997. Analysing multidirectional wave spectra: a tentative classification of available methods, Proceedings IAHR Seminar on Multidirectional Waves and their Interaction with Structures, 27th IAHR Congress, San Francisco (USA) 1997 pp. 131–154.

Borgman, L.E., 1969. Directional spectra models for design use, Offshore Technology Conference, Houstan, Texas, vol. 1 1969 pp. 721–741.

Briggs, M.J., Thompson, E.F., Vincent, C.L., 1995. Wave diffraction around breakwater. Journal of Waterway, Port, Coastal, and Ocean Engineering 121 (1), 23–35.

Chaplin, J.R., Subbiah, K., Irani, M., 1995. Loading on a vertical cylinder in multidirectional waves. Journal of Offshore Mechanics and Arctic Engineering 117, 151–158.

Donelan, M.A., Hamilton, J., Hui, W.H., 1985. Directional spectra of wind-gathered waves. Philosophical Transactions of the Royal Society of London, Series A 315, 509–562.

Forristall, G.Z., Ewans, K.C., 1998. Worldwide measurements of directional wave spreading. Journal of Atmospheric and Oceanic Technology 15, 440–469.

Haring, R.E., Heideman, J.C., 1980. Gulf of Mexico rare wave return periods. Journal of Petroleum Technology 265, 35–47.

Hashimoto, N., Konube, K., 1986. Estimation of directional spectra from the maximum entropy principle, Proceedings of the Fifth International Conference on Offshore Mechanics and Arctic Engineering, Tokyo, Japan 1986 pp. 80–85.

Hasselmann, D.E., Dunkel, M., Ewing, J.A., 1980. Directional wave spectra observed during JONSWAP 1973. Journal of Physical Oceanography 10, 1264–1280.

Heideman, J.C., Weaver, O.T., 1992. Static wave force procedure for platform design, Civil Engineering in the Oceans 5, International Conference, November, Texas, USA 1992 pp. 496-517.

Hogedal, M., Skourup, J., Burcharth, H.F., 1994. Wave forces on a vertical smooth cylinder in directional waves, Proceedings of the Fourth International Offshore and Polar Engineering Conference, Osaka, Japan, April 10–15, vol. III 1994 pp. 218–223.

Isobe, M., Konda, K., Horikawa, K., 1984. Extension of MLM for estimating directional wave spectrum, Proceedings Symposium on Description and Modelling of Directional Seas, Lyngby (Denmark), June 18–20, paper no. A-6 1984.

ISO/TC67/SC7/WG3, ISO/DIS 19901-1 (draft), 2002. Petroleum and natural gas industries—specific requirements for offshore structures. Part 1. Metocean design and operating condition.

Jonathan, P., Taylor, P.H., Tromans, P.S., 1994. Storm waves in the northern North Sea, Seventh International Conference on the Behaviour of Offshore Structures. Massachusetts Institute of Technology, Boston, MA, pp. 481-494.

Krogstad, H.E., 1988. Maximum likelihood estimation of ocean wave spectra from general arrays of wave gauges. Modelling, Identification and Control 9, 81–97.

Krogstad, H.E., Barstow, S.F., 1999. Directional distributions in ocean wave spectra. Proceedings of the Ninth International Offshore and Polar Engineering Conference, Brest, France, Vol. III, pp. 79–86.

Linfoot, B., Wolfram, J., Stansell, P., 2000. Modulational interactions of broad-band gravity waves observed during North Sea storms, Rogue Waves 2000, Brest, France 2000 pp. 215–220.

Longuet-Higgins, M.S., Stewart, R.W., 1960. Changes in the form of short gravity waves on long waves and tidal currents. Journal of Fluid Mechanics 8, 565–583.

Longuet-Higgins, M.S., Cartwright, D.E., Smith, N.D., 1963. Observations of the directional spectrum of sea waves using the motions of a floating buoy, Ocean Wave Spectra. Prentice-Hall, Englewood Cliffs, NJ pp. 111–136.

Lygre, A., Krogstad, H.E., 1986. Maximum entropy estimation of the directional distribution in ocean wave spectra. Journal of Physical Oceanography 16, 2052–2060.

Massel, S.R., Brinkman, R.M., 1998. On the determination of directional wave spectra for practical applications. Applied Ocean Research 20, 357–374.

Mitsuyasu, H., Tasai, F., Suhara, T., Mizuno, S., Ohkuso, M., Honda, T., Rikishi, K., 1975. Observations of the directional spectrum of ocean waves using a cloverleaf buoy. Journal of Physical Oceanography 5 (2), 750–760.

Nortek, As. 2000. Nortek velocimeter—operations manual, Norway (www.nortek-as.com).

Rogers, D., King, B.G., 1997. Wave generation using ocean and wave. Users Manual Ver. 3.61, Edinburgh Designs Ltd, UK.

Stockwell, R.G., Mansinha, L., Lowe, R.P. 1996. Localization of the complex spectrum: The S Transform, IEEE, T. Sig. Pro., 44. pp. 998–1001

Tucker, M.J., 1991. Waves in Ocean Engineering—Measurement, Analysis, Interpretation. Ellis Horwood, England.

Tucker, 1996, 1996. The wave spreading factor in U.K. waters, Offshore Technology Paper, No.OTO 96025. HMSO, London.

Wolfram, J., Venugopal, V., 2003. Crest height statistics of storm waves in deep water. Journal of Engineering for the Maritime Environment M4, 217 pp. 213–229.

Wolfram, J., Linfoot, B.T., Venugopal, V., 2001. Evolution of wave characteristics due to storms in North Sea, International Conference in Ocean Engineering. Indian Institute of Technology, Madras, India pp. 109–114.

Zhang, J., Melville, W.K., 1990. Evolution of weakly nonlinear short waves riding on long gravity waves. Journal of Fluid Mechanics 214, 321–583.

Zhang, J., Chen, L., Ye, M., Randall, R.E., 1996. Hybrid wave model for unidirectional irreular waves. Part I. Theory and numerical scheme. Applied Ocean Research 18, 77–92.

Zhang, J., Yang, J., Wen, J., Prislin, I., Hong, K., 1999. Deterministic wave model for short-crested ocean waves. Part I. Theory and numerical scheme. Applied Ocean Research 21, 167–188.